J. Morris
Department of Mechanical Engineering,
Massachusetts Institute of Technology,
Cambridge, MA 02139

E. P. Ingenito

L. Mark

Division of Pulmonary
and Critical Care Medicine,
Brigham and Women's Hospital,
Boston, MA 02115

R. D. Kamm

M. Johnson

Department of Mechanical Engineering,
Massachusetts Institute of Technology,
Cambridge, MA 02139.

Dynamic Behavior of Lung Surfactant

We have previously developed an adsorption-limited model to describe the exchange of lung surfactant and its fractions to and from an air–liquid interface in oscillatory surfactometers. Here we extend this model to allow for diffusion in the liquid phase. Use of the model in conjunction with experimental data in the literature shows that diffusion-limited transport is important for characterizing the transient period from the start of oscillations to the achievement of steady-state conditions. Matching previous data shows that upon high levels of film compression, large changes occur in adsorption rate, desorption rate, and diffusion constant, consistent with what one might expect if the subsurface region was greatly enriched in DPPC. Collapse of the surfactant film that occurs during compression leads to a significant elevation of surfactant concentration immediately beneath the interface, consistent with the subsurface depot of surfactant that has been postulated by other investigators. Modeling studies also uncovered a phenomenon of surfactant behavior in which the interfacial tension remains constant at its minimum equilibrium value while the film is compressed, but without collapse of the film. The phenomenon was due to desorption of surfactant from the interface and termed ''pseudo-film collapse.'' The new model also gave improved agreement with steady-state oscillatory cycling in a pulsating bubble surfactometer. [DOI: 10.1115/1.1336146]

Keywords: Surface Tension, Dynamic, Model, Surfactometer, Diffusion, Adsorption

Introduction

The behavior of surfactant in the lung is frequently characterized in vitro using a bubble surfactometer [1–4]. In such a device, a small bubble within a bulk suspension containing surfactant is expanded and contracted in an oscillatory fashion, while the surface tension of the interface is dynamically determined by either by measuring the pressure drop across the bubble surface (pulsating bubble surfactometer [5]) or by analyzing the bubble shape (captive bubble surfactometer [6]). We have previously developed an analytical model that predicts many of the features characteristic of the oscillatory surface tension versus interfacial area profiles that are obtained experimentally in such bubble surfactometers [7,8]. This adsorption-limited model, that characterizes the exchange of surfactant from the bulk suspension to and from the air–liquid interface and allows for phase changes in the latter, has been used to characterize the dynamic surface tension behavior of TA surfactant [7], lung surfactant, DPPC, and the different surfactant fractions that make up lung surfactant [8].

While this model has worked well[1] to characterize the steady-state, oscillatory dynamics of the transport of lung surfactant into and out of the air/liquid, our first attempts to use this model to characterize the initial transient behavior that occurs upon initiation of pulsation, before steady-state was reached, were less successful. Our previous model showed steady-state behavior was reached, in general, after only a few oscillatory cycles. However, data from Schürch et al. [3] on the dynamic surface tension behavior of Curosurf surfactant, a derivative of porcine lung surfactant, showed significant transient effects that continued over many cycles (>20 cycles at 20 cycles/min). Our goal here is to extend our model to allow for a characterization of these transient effects.

Our adsorption-limited model assumes the surfactant in the liquid to be spatially uniform in concentration. As such, the only transient behavior in the model comes from the time-scale required to saturate the interface with surfactant, which, at high bulk concentrations, is shorter than the period of oscillation of interfacial area in these studies. However, as Schürch et al. have observed transient behavior that extended over many cycles, we conclude that transport of surfactant from the bulk to the interface can be diffusion-limited under some conditions.

To examine this possibility, we here extend our model to include the effects of diffusion and compare our model results to both transient and steady-state oscillatory data. This extended model well characterizes the transient data of Schürch et al., as well as showing even better agreement with steady-state oscillatory behavior of surfactant than did our adsorption-limited model. Furthermore, the model predicts, under some conditions, the formation of a high-concentration sublayer of surfactant immediately beneath the interface, in agreement with reports of other investigators [9,3]. Finally, our model predicts a form of surfactant dysfunction that resembles the film collapse that occurs at that occurs at high levels of compression of the surfactant [10,11,9] but is in fact due to a desorption limitation.

Computational Model

We here model the process by which surfactant is transported from the bulk suspension to the time-varying interface of the bubble (radius $R(t)$). We follow the approach of Chang and Franses [12] using the convective diffusion equation in a coordinate system moving relative to the moving interface, $x(t)=r-R(t)$, where r is radial distance from the center of the bubble:

$$\frac{\partial C(x,t)}{\partial t}+v_{rel}(x,t)\frac{\partial C(x,t)}{\partial x}=\frac{D}{(x+R(t))^2}\frac{\partial}{\partial x}\left[(x+R(t))^2\frac{\partial C(x,t)}{\partial x}\right] \quad (1)$$

where $C(x,t)$ is the concentration of surfactant in the bulk, D the diffusion coefficient of the surfactant in the bulk, and v_{rel} is the velocity of the fluid relative to the interface:

[1]It should be noted that while our model predictions for the shape of the surface area versus interfacial area loops are in very good qualitative agreement with what is seen experimentally, its predictions for the peak surface tension are consistently low for the higher bulk concentration. We have previously attributed this discrepancy to the phenomenon of film rupture that is not currently in our model [7].

Contributed by the Bioengineering Division for publication in the JOURNAL OF BIOMECHANICAL ENGINEERING. Manuscript received by the Bioengineering Division August 31, 1999; revised manuscript received August 24, 2000. Associate Editor: S. E. Rittgers.

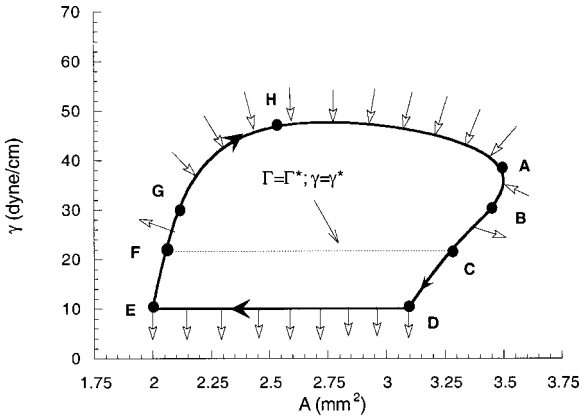

Fig. 1 Schematic of steady-state surface tension γ versus bubble area *A* loop demonstrating surfactant transfer mechanisms for each loop segment: kinetic adsorption (between G and B along top of loop) or desorption (segments FG and BC) for $\gamma > \gamma^*$ (regime *i*), insoluble monolayer for $\gamma_{min} < \gamma < \gamma^*$ (segments CD and EF) (regime *ii*), and film collapse as the area is lowered beyond the point where γ_{min} is reached (between D and E) (regime *iii*). The inward and outward arrows represent adsorption/desorption/film-collapse of surfactant by the monolayer. Loop direction is clockwise.

$$v_{rel}(x,t) = \left[\left(\frac{R(t)}{x + R(t)} \right)^2 - 1 \right] \frac{dR(t)}{dt}$$

We require an initial condition and two boundary conditions to solve this differential equation. Generally we assume uniform surfactant concentration (C_{bulk}) in the liquid at $t = 0$:

$$C(x,0) = C_{bulk} \tag{2}$$

The suspension surrounding the bubble was modeled as infinite in spatial extent such that transport of surfactant to or from the interface did not affect the concentration of surfactant in the bulk far from the interface, hence:

$$C(\infty,t) = C_{bulk} \tag{3}$$

Finally, we require a boundary condition at the air–liquid interface. This was specified as a flux condition passing from the liquid (at $x = 0$) into or out of the interface.

$$\frac{d[A(t)\Gamma(t)]}{dt} = A(t) D \frac{\partial C(0,t)}{\partial x} \tag{4}$$

Here, $A(t) = 4\pi R^2(t)$ and $\Gamma(t)$ is the interfacial concentration of surfactant. It is through this exchange condition that we relate the current model to our previous model of adsorption limited transport of surfactant to the interface. That model characterizes surfactant transport to and from the interface in terms of three distinct surface concentration regimes (see Fig. 1) [7]:

(i) $\Gamma < \Gamma^*$: *Langmuir adsorption regime* (segment *FC* on Fig. 1). Γ^* is the maximum interfacial concentration of surfactant that can be achieved at equilibrium as bulk phase concentration (C_{bulk}) is increased. In this regime, adsorption and desorption are assumed to occur according to the Langmuir relationship:

$$\frac{d(A\Gamma)}{dt} = A[k_1 C(0,t)(\Gamma^* - \Gamma) - k_2 \Gamma] \tag{5a}$$

where k_1 is the adsorption coefficient and k_2 the desorption coefficient. This differs from our previous model by allowing adsorption to depend on the concentration of surfactant in the liquid at $x = 0$, which now differs from C_{bulk}.

(ii) $\Gamma^* < \Gamma < \Gamma_{\max}$,: *Insoluble regime* (segments *CD* and *EF* on Fig. 1). $\Gamma_{\max}$ is the maximum interfacial concentration of surfactant that can be achieved during lateral compression of surface active material at the interface. In this regime, the surfactant is modeled as insoluble, i.e., it does not exchange surface active material with the liquid phase.

$$d(A\Gamma)/dt = 0 \tag{5b}$$

(iii) $\Gamma = \Gamma_{\max}$ *''Film collapse''regime* (segment *DE* on Fig. 1). We define ''film collapse'' as occurring when the surfactant molecules are packed as tightly as possible in the interface, and a further decrease of interfacial area is accompanied by an ejection of material from the interface to the liquid at $x = 0$.

$$d(A\Gamma)/dt = -\Gamma_{max} dA/dt \tag{5c}$$

Surface tension reaches its minimum value ($\gamma_{\min}$) at this point, and remains constant as the film is further compressed.

Equations (1)–(5) can be solved for the interfacial concentration as a function of time for a given history of the interfacial area. This is found assuming spherical geometry with the bubble volume prescribed as:

$$V(t) = V_{mean} + \frac{V_{cycle}}{2} \sin\left(2\pi\omega t - \frac{\pi}{2} \right) \tag{6}$$

To find surface tension (γ) as a function of time, we prescribe an isotherm that relates surface tension to interfacial concentration as was done previously [7,8]. The functional form chosen for the isotherm—two straight lines with a common point at $\Gamma = \Gamma^*$, $\gamma = \gamma^*$—is entirely characterized by the two slopes, $d\gamma/d\Gamma = m_1$ for $\Gamma/\Gamma^* < 1$ and $d\gamma/d\Gamma = m_2$ for $\Gamma/\Gamma^* > 1$. We have previously used more complicated isotherms and found little influence on predicted dynamic profiles [13].

Numerical Solution. A brief summary of the numerical methods used are provided here, the details of which are found elsewhere [14]. The equations are discretized using a control volume approach that includes a second-order spatial differencing scheme for the diffusive term, a first-order upwind difference scheme for convective terms, and an implicit Euler scheme in time [15]. The bulk is spatially discretized into nodes, with each node being at the center of its control volume. The first node, representing the subsurface, is at a distance $\Delta x/2$ from the interface, with each subsequent node Δx further. The subsurface is specified to be $\Delta x/2$ from the interface instead of on the interface as this arose naturally from the differencing scheme allowing a more accurate calculation of the interfacial mass flux [15].

Boundary condition (5*a*) involves a nonlinear term (ΓC) that precludes an implicit differencing scheme. To facilitate a more accurate characterization of this term, the liquid and interfacial surfactant concentrations were rewritten in terms of differences between the current and next time step:

$$\Delta c(x,t+\Delta t) \equiv c(x,t+\Delta t) - c(x,t)$$

$$\Delta\Gamma(t+\Delta t) \equiv \Gamma(t+\Delta t) - \Gamma(t)$$

leading to

$$c(x=0,t+\Delta t)\Gamma(t+\Delta t) \doteq c(x=0,t)\Gamma(t) + \Delta c(x=0,t+\Delta t)\Gamma(t) + c(x=0,t)\Delta\Gamma(t+\Delta t)$$

where the second-order term has been dropped. This approximation is substituted into Eq. (5*a*), thus linearizing the equation and allowing an implicit differencing scheme.

The spatial increment, $\Delta x = \sqrt{D\Delta t}/2$, is one-half of the characteristic diffusion length, so that the mesh will automatically be fine enough to resolve diffusional processes. The time increment, Δt, is set to be $1/(N_{SC}\omega)$, where ω is the cycling frequency and N_{SC} is the number of time steps per cycle. For our modeling, $N_{SC} = 1000$; larger values (smaller Δt and Δx) have no effect on the results.

Distance to the bulk, L_∞, was chosen to be five times the greater of the adsorptive or diffusive characteristic length scale for the process, such that the boundary condition, (3), can be applied.

The number of spatial nodes, N_{SN}, was chosen such that $N_{SN} = L_\infty / \Delta x$. The diffusive and adsorptive lengths, respectively, normalized by Δx, are:

$$\frac{l_D}{\Delta x} = \frac{\sqrt{Dt}}{\Delta x} = 2\sqrt{N_{SC} N_C} \tag{8}$$

$$\frac{l_A}{\Delta x} = \frac{1}{\Delta x}\frac{\Gamma^*}{C_{bulk}} = \frac{2\sqrt{N_{SC}}}{\sqrt{D/\omega}}\frac{\Gamma^*}{C_{bulk}} \tag{9}$$

where t is the total time of simulation and N_C the number of cycles of simulation ($t = N_{SC} N_C \Delta t$).

The Courant number, $v_{\text{rel}} \Delta t / \Delta x$, and the numerical Peclet number, $v_{\text{rel}} \Delta x / D$, are both ensured to be less than one for $x < l_D$ and $x < l_A$. In a few cases, this requires an increase in N_{SC}.

The discretized equations are assembled into a tri-diagonal matrix and solved [16]. We verified our numerical scheme by comparing to our results to (*i*) analytical solutions to unsteady diffusion into a semi-infinite space and (*ii*) published results of an alternate pulsating bubble model [12]. In the first case, our results matched within 0.1 percent accuracy and in the second, our results matched as closely as could be determined from the figures presented in that work [14]. We also checked to make sure that total surfactant was conserved during a simulation and found that the error was always less than 0.1 percent [14]. For those runs that were extended to a ''steady-state,'' we continued the simulation until the surface tension at all points in the cycle changed by less than 0.15 dynes/cm from one cycle to the next.

Parameter Values. Characterization of surfactant behavior by our model requires the following parameters: Γ^*, Γ_{max}, γ^*, γ_{min}, D, k_1, k_2, m_1 and m_2. Γ^* and m_1 are not independent parameters and can be determined from the others [8] as:

$$m_1 = 70 \text{ dynes/cm-}\gamma^* \tag{10}$$

and

$$\Gamma_{max} = \Gamma^*[1 + (\gamma^* - \gamma_{min})/m_2] \tag{11}$$

leaving seven independent parameters. We largely followed our previous methods [8] to determine these parameters.

Γ^* was assumed to be equal to 3×10^{-7} g/cm^2 in all of our studies [17]. γ^* is a measured parameter determined to be the lowest surface tension that can be obtained under equilibrium conditions as the bulk concentration of surfactant is increased. γ_{min} is the lowest surface tension achievable under dynamic compression which for the surfactants considered here was always assumed to be 1 dyne/cm. m_2 is determined from the slope $d\gamma/dA$ for $\Gamma^* < \Gamma < \Gamma_{max}$, [8]. As the ratio of k_1/k_2 has been largely constant in all of our studies to date, we used the previously determined value of 1.2×10^5 ml/g in the simulations reported here. Finally, we assumed that $\Gamma(t=0) = \Gamma_{eq}$ where $\Gamma_{eq}/\Gamma^* = k_1 C_{bulk}/(k_1 C_{bulk} + k_2)$ [7].

The remaining two parameters, D and k_1 were determined from the transient and oscillatory surface tension versus interfacial area profiles as described in the results section. A correction was necessary to the value of k_1 when Γ approached Γ^*. Our model makes the simplistic assumption that when the surfactant in the interface undergoes a phase transition from regime (*i*) to regime (*ii*), the values of these two parameters drop discontinuously to zero when $\Gamma = \Gamma^*$ [7]. This can lead to a nonphysical trapping of Γ just below Γ^*. We discuss this phenomenon in considerably more detail in the section on ''pseudo-film collapse.'' To avoid this numerical artifact, we allowed k_1 and k_2 to drop continuously to zero:

$$k_1(\Gamma) = \beta(\Gamma) K_1$$
$$k_2(\Gamma) = \beta(\Gamma) K_2 \tag{12}$$

where

$$\beta(\Gamma) = \begin{cases} 1 & \dfrac{\Gamma}{\Gamma^*} < 0.96 \\ 25\left(1 - \dfrac{\Gamma}{\Gamma^*}\right) & 0.96 < \dfrac{\Gamma}{\Gamma^*} < 1 \\ 0 & \dfrac{\Gamma}{\Gamma^*} > 1 \end{cases}$$

and K_1 and K_2 are constants. Allowing this linear decrease in k_1 for $0.96 < \Gamma < 1$ is admittedly somewhat arbitrary, but it eliminated the numerical artifact, and altering the value of Γ/Γ^* at which this linear decrease was begun did not significantly affect our results, except, of course, in the vicinity of the phase transition between regime (*i*) and regime (*ii*) [14].

Finally, we should note here that there are several sources of uncertainty in our determination of the best fit parameters that match a particular data set. These uncertainties including experimental uncertainty, the choice of what aspects of the experimental data to match, and the simplicity of our model that limits our ability to match all aspects of the data sets. In general, we have found that our model to give good qualitatively agreement with experimental data [7,8]. However, the quantitative values of the parameters that are determined, particularly k_1 and D, should be viewed as semi-quantitative measures with uncertainties of roughly 1/2 of a log unit.

Results

We used this extended model to (*i*) compare to the transient data of Schürch et al. [3], in a captive bubble surfactometer that had first motivated the need to extend the model and (*ii*) compare to our previous work on steady-state oscillatory data in a pulsating bubble surfactometer. We also found a new phenomenon we term ''pseudo-film collapse'' that is described below.

Comparison to Data of Schürch et al. [3]. The data of Schürch et al. provided three types of experiments that we simulated using our diffusional model: surface tension versus time for a constant-area adsorption of surfactant to a fresh bubble (Fig. 2(A)), surface tension versus interfacial area during dynamic cycling of a bubble (Figs. 3(A–C)), and surface tension versus time for constant-area surfactant adsorption onto an interface at maximum expansion after the bubble has been cycled a given number of times (Fig. 4(A)). These experiments were done with Curosurf surfactant (porcine lipid extract) at a bulk concentration of 1 mg/ml and, where applicable, at a cycling frequency of 20–30 cycles/min.

Figure 2(A) shows the nearly immediate drop in surface tension that occurs in a freshly formed bubble. This experiment shows that the surface tension falls almost instantaneously from $\gamma_{water} \approx 70$ dynes/cm, so rapidly in fact that the highest reported surface tension in this static equilibration was 30–35 dynes/cm. In approximately one second, the surface tension has reached equilibrium at $\gamma_{eq} \approx 25$ dynes/cm.

D and K_1 cannot be separately determined from the data in Fig. 2(A) since only a single time constant can be ascertained. However, using our model, we can determine that $D > 5 \times 10^{-8}$ cm^2/s and $K_1 > 1.0 \times 10^5$ ml/(g·min) in order to be consistent with the decay rate shown in Fig. 2(A). Figure 2(B) shows the model predictions for a diffusion coefficient of $D = 10^{-6}$ cm^2/s (that of individual DPPC molecules [17]) and $K_1 = 6 \times 10^5$ ml/(g·min) (our previously determined value for calf lung surfactant [8]).

Figure 3 shows the shape of the dynamic γ–A profile for the first (3(A)), second (3(B)), and twentieth cycles (3(C)). Schürch et al. reported that ''no noticeable change'' in the shape of the γ–A loop was observed as testing was extended from 20 to 50 cycles. As mentioned above, our previous model, without including the effects of diffusion, would predict steady-state behavior after only a few cycles and thus would be unable to match the data reported by Schürch et al.

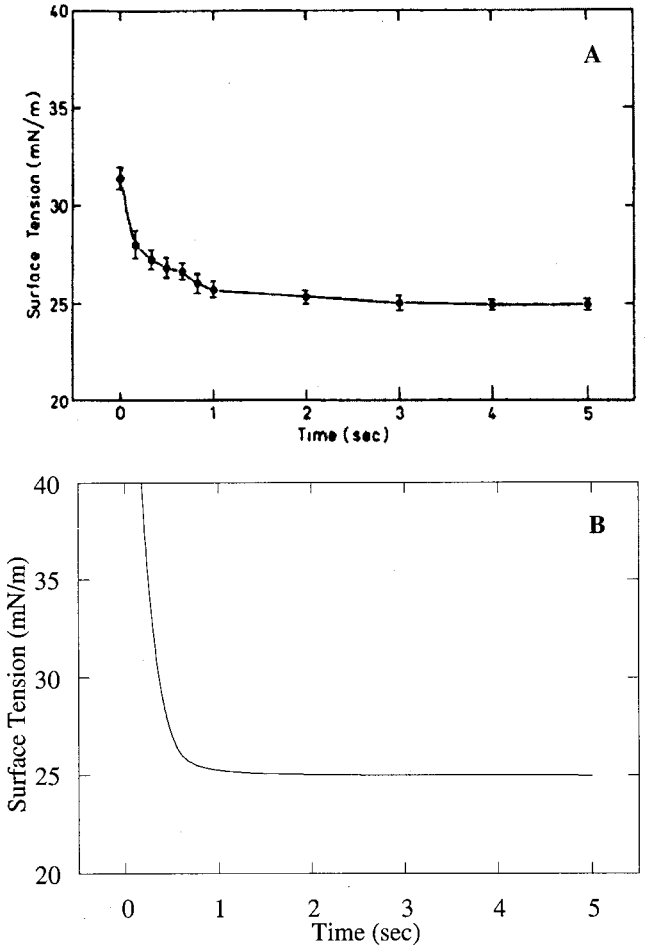

Fig. 2 Surface tension versus time during constant-area adsorption of surfactant to freshly formed bubble. (A) Experiment data [3]; (B) model predictions with $D=10^{-6}$ cm^2/s and $K_1=6\times10^5$ ml/(g·min).

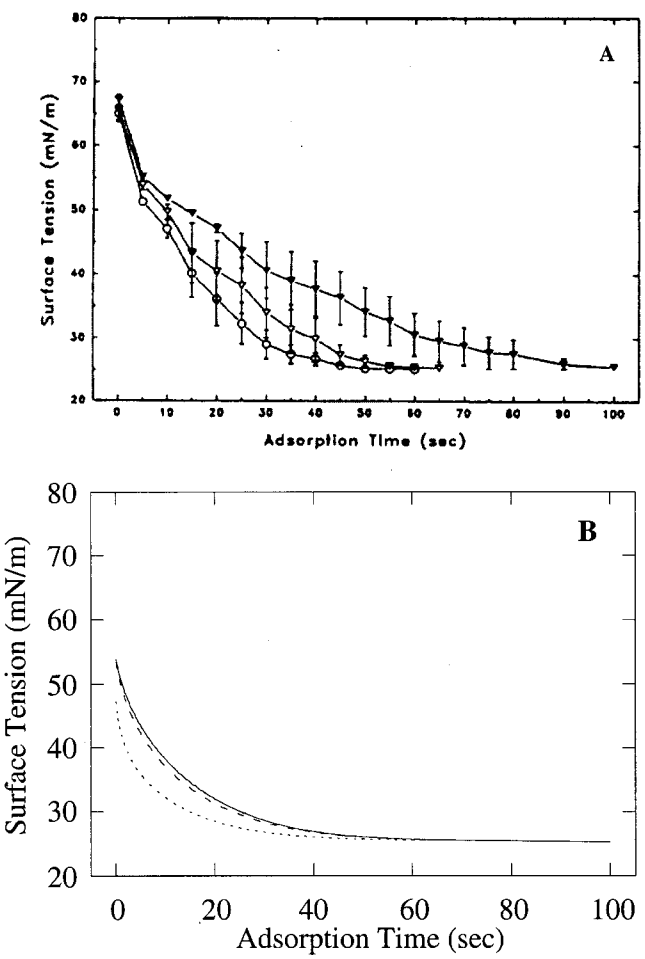

Fig. 4 Constant-area adsorption of 1 mg/ml Curosurf at maximum bubble area after consecutive dynamic cycles (same condition as for Fig. 3). (A) Experiment data [3] with cycling stopped after 1 cycle (open circles), 20 cycles (open triangles), or 50 cycles (filled triangles); (B) model predictions with $D=10^{-9}$ cm^2/s and $K_1=0.07\times10^5$ ml/(g·min) for these same conditions.

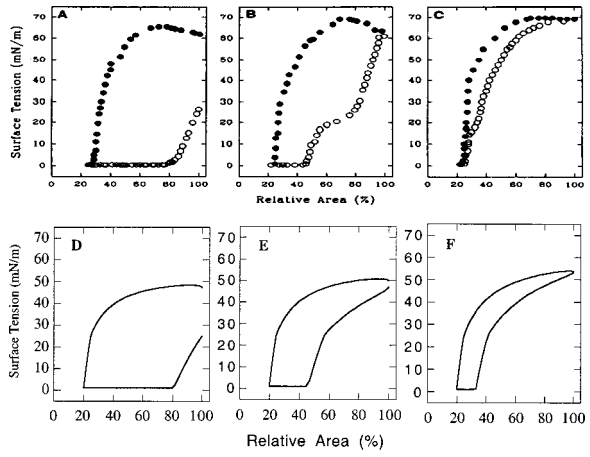

Fig. 3 Dynamic surface tension–interfacial area for first few cycles for Curosurf (porcine lipid extract) at 1 mg/ml and 20–30 cycles/min. (A–C) Experimental loops [3] are shown for cycle 1 (A), cycle 2 (B), and cycle 20 (C); open circles denote compression; filled circles, expansion. (D–F) Diffusional model predictions for $D=10^{-9}$ cm^2/s and $K_1=0.07\times10^5$ ml/(g·min); other parameters as specified in the text (25 cycles/min).

To match the model to the data, γ^* was estimated as 25 dynes/cm and m_2 as 100 dynes/cm using the methods described above and data from Figs. 2(A) and 3(A). D and K_1 were determined as those values that gave the best agreement for the interfacial area at which the surface tension versus interface area loop first entered the film-collapse regime (point D of Fig. 2) [8] for the second experimental loop (Fig. 3(B)). Specifically, we considered a range of diffusion coefficients ranging from a somewhat arbitrary lower limit of 1×10^{-11} cm^2/s to an upper limit of that of individual DPPC molecules (1×10^{-6} cm^2/s [17]), and for each value of D, found the optimal value of K_1. The results are shown as the filled symbols in Fig. 5.

Values of $D>1\times10^{-9}$ cm^2/s lead to steady-state behavior being reached well before the twentieth cycle, contrary to the reported experimental data. Notably, the values of D and K_1 necessary to match Fig. 2(A) do not fall on the curve traced out by the filled circles in Fig. 5, a point we return to in the discussion. Figures 3(D–F) show model matches for Figs. 3(A–C) with $D=1\times10^{-9}$ cm^2/s and $K_1=0.07\times10^5$ ml/g/min. These values were picked because they not only give good agreement between model and data for Fig. 3, but also for Fig. 4, as we shall see.

Figure 4(A) shows the decrease in surface tension as a function of time during constant-area surfactant adsorption onto an interface at maximum expansion after the bubble has been cycled for

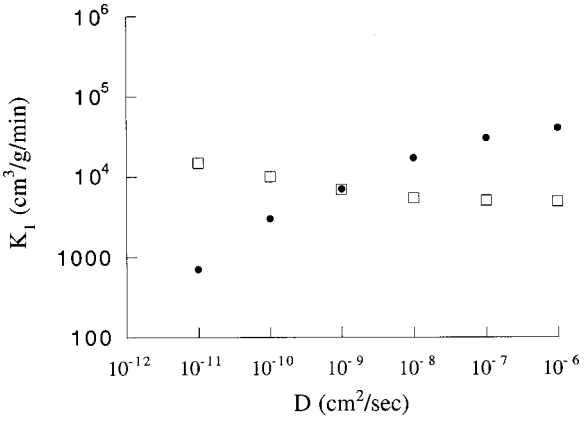

Fig. 5 Values of K_1 (ml/g·min) and D (cm^2/s) necessary to match film-collapse area of Fig. 3(B) (filled circles) or to match time-constant for adsorption shown in Fig. 4(A) (open squares)

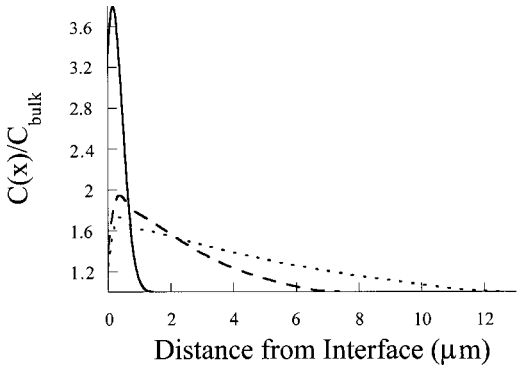

Fig. 7 Predictions of surfactant concentration profile in the liquid at maximum bubble area after 1 (solid), 20 (dashed), or 50 (dotted) cycles for the dynamic cycling described in Fig. 3

1, 20, or 50 cycles (Fig. 4(A)). It is striking that the time scale for this drop of surface tension is two orders of magnitude longer than the time scale for surface tension equilibration for a freshly formed bubble (Fig. 2(A)). As with Fig. 2(A), since the data provide only a single time constant, unique values of D and K_1 cannot be determined. However, following the procedure used to match the data in Fig. 3(B), we can again find optimal values of K_1 for $1\times10^{-11}<D<1\times10^{-6}$ cm^2/s, in this case, matching the time constant seen in Fig. 4(A). The result is shown in Fig. 5 (open symbols).

The intersection of the set of open and closed symbols in Fig. 5 specifies the values of D and K_1 that fit both Figs. 3(A–C) and Fig. 4(A). Figure 4(B) shows model predictions for the conditions of Fig. 4(A) with $D=1\times10^{-9}$ cm^2/s and $K_1=0.07\times10^5$ ml/g/min. It is notable that the diffusion coefficient that matches both of these data sets is much lower than that of individual DPPC molecules, as will be discussed later.

Using these selected model parameters, we can predict the concentration profile of surfactant in the liquid, and how this profile changes with time. Figure 6 shows $C(x=0,t)$ and illustrates the very high concentration of surfactant in the subsurface region achieved during compression on each cycle in Fig. 3(A–C), especially at the beginning of the cycling. Note in Fig. 7 the thin region in which this high concentration of surfactant occurs and that this depot diffuses away only slowly from the interfaces. This

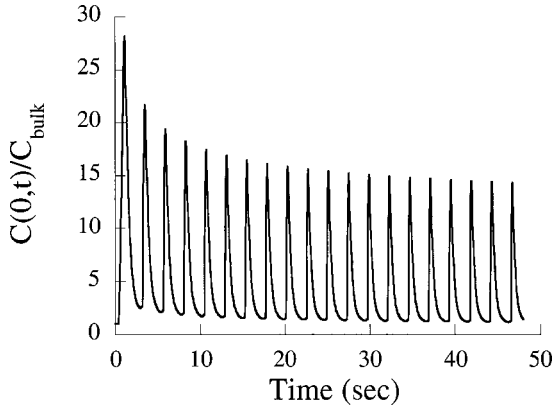

Fig. 6 Predictions for surfactant concentration in the subsurface region immediately underlying the interface, $C(0,t)$, for the dynamic cycling described in Fig. 3

is likely the subsurface surfactant depot that has been discussed by other investigators [9] and was postulated by Schürch et al. [3] based upon their data.

Steady-State Oscillatory Data in a Pulsating Bubble Surfactometer. We here use our extended model to compare to steady-state oscillatory data (1, 20, and 100 cycles/min; 0.01, 0.1, and 1 mg/ml) that we have previous published for calf lung surfactant in a pulsating bubble surfactometer [8]. We only consider steady-state data, as there have been questions raised in the literature concerning potential surfactant leakage out of the pulsating bubble surfactometer during the transient period before steady-state behavior is reached [18]. Figures 8(A–C) show our previous data [8] and Figs. 8(D–F) show the best parameter match of our previous adsorption-limited model [8].

To match these data with our extended model, we used the best-fit parameters determined by Ingenito et al. (as described in the methods section, with $K_1=6\times10^5$ ml/g/min and $m_2=140$ dynes/cm) and allowed D to vary between 1×10^{-9} cm^2/s (the best-fit value that matched the data of Schürch et al.) and 10^{-6} cm^2/s (individual DPPC molecules).

Figure 9(A–C) show the model predictions for $D=1\times10^{-6}$ cm^2/s, and Figs. 9(D–F) show model predictions for $D=1\times10^{-9}$ cm^2/s. The former not only show better agreement with the data than does the latter (especially at 1 mg/ml), but also show better agreement (see the solid line in the low bulk concentration graphs) than did our previous adsorption-limited model (Figs. 8(D–F)). We also allowed $K_1=0.07\times10^5$ ml/g/min (the best fit value that matched the data of Schürch et al.) and again found (not shown) that this adsorption constant was much too low to match our steady-state data in the pulsating bubble surfactometer, a point we return to in the discussion section.

We use these optimal model parameters to make predictions concerning the concentration of surfactant in the liquid. Figure 10 shows the concentration of surfactant in the subsurface region, $c(x=0,t)$ for calf surfactant in a pulsating bubble surfactometer. Note that the concentration of surfactant in the subphase is much less than that predicted for the experimental conditions examined by Schürch et al. (Fig. 7) and reaches steady state much more quickly.

Pseudo-Film Collapse. As mentioned in the methods section, we applied a correction to the values of k_1 and k_2 when Γ approached Γ^* so that these parameters did not drop discontinuously to zero when phase transition occurred at $\Gamma=\Gamma^*$. This prevented what we at first thought to be a nonphysical trapping of Γ just below Γ^*.

We call this trapping ''pseudo-film collapse,'' since it exhibits the same $\gamma-A$ characteristic as does true film collapse seen in regime (iii), namely, that surface tension remains relatively con-

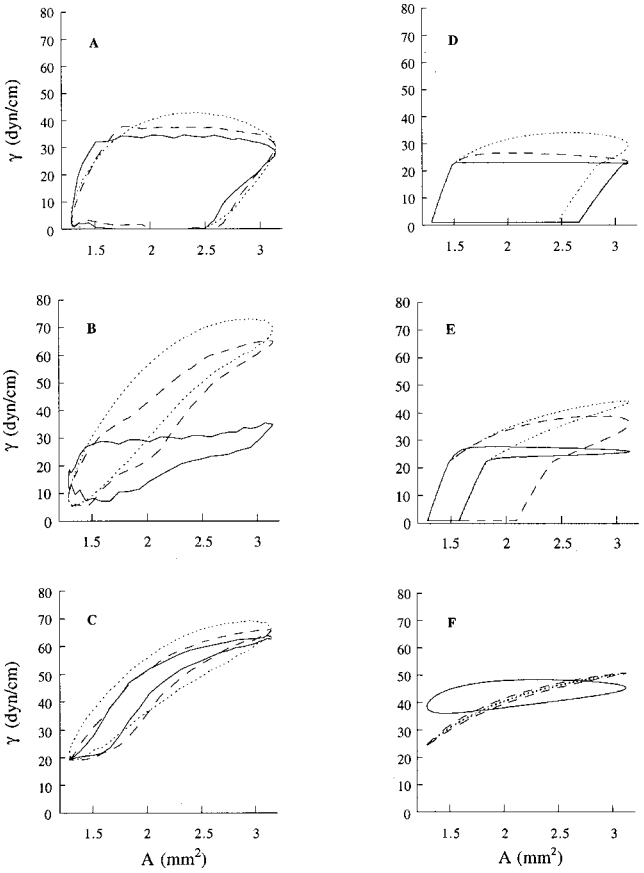

Fig. 8 Steady-state surface tension versus interfacial area loops for calf lung surfactant measured during pulsating bubble surfactometry. (A, D) 1 mg/ml, (B, E) 0.1 mg/ml, (C, F) 0.01 mg/ml; solid: 1 cycle/min, dashed: 20 cycles/min, dotted: 100 cycles/min. (A–C) Experimental data [8]; (D–F) model predictions with $K_1=6\times10^5$ ml/(g·min) and $D=\infty$ (adsorption-limited model) and other parameters as described in text.

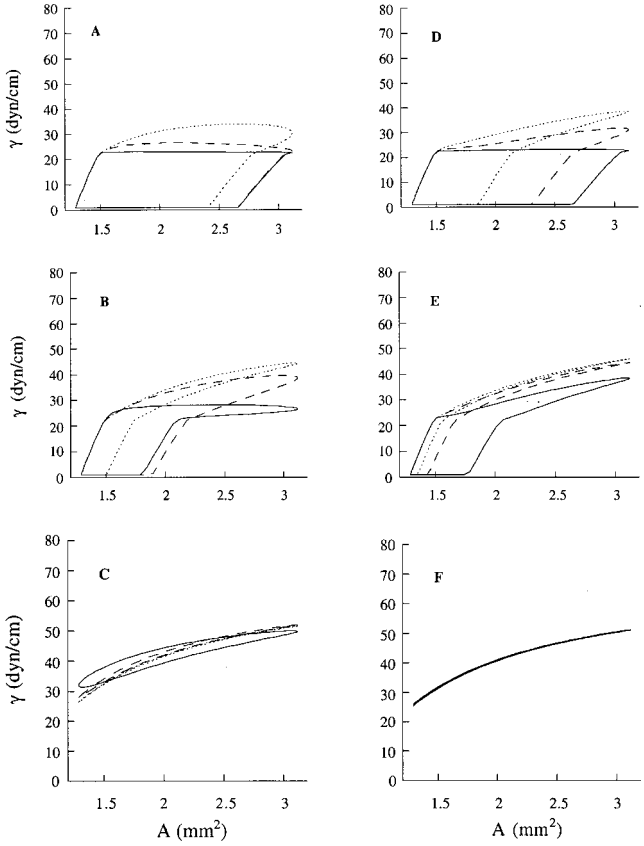

Fig. 9 Model prediction for steady-state surface tension versus interfacial area loops for calf lung surfactant measured during pulsating bubble surfactometry; $K_1=6\times10^5$. (A, D) 1 mg/ml, (B, E) 0.1 mg/ml, (C, F) 0.01 mg/ml; solid: 1 cycle/min, dashed: 20 cycles/min, dotted: 100 cycles/min. (A–C): $D=1\times10^{-6}$ cm²/s; (D–F): $D=1\times10^{-9}$ cm²/s; other parameters as described in text.

stant as interfacial area is reduced. However, it occurs near $\gamma=\gamma^*$ instead of $\gamma=\gamma_{\min}$. Pseudo-film collapse is a result of the bubble being unable to reach sufficient interfacial surfactant concentration to enter the insoluble regime. Two opposing mechanisms are acting to alter the interfacial concentration as Γ approaches Γ^*: desorption acts to lower the interfacial concentration by ejecting molecules from the interface, while the compression of the bubble raises the interfacial concentration by compacting the interfacial film. To exhibit pseudo-film collapse, the rate of change of the interfacial concentration must be negative for some Γ in the compression cycle. Using Eq. (5*a*), we find that criterion for pseudo-film collapse during the compression cycle to be:

$$k_2\Gamma > k_1 C_s(\Gamma^*-\Gamma) - \frac{\Gamma}{A}\frac{dA}{dt} \tag{13}$$

If the cycling frequency is sufficiently high, this criterion will not be met, and Γ will rise to Γ^*. Once Γ^* is reached, k_2 drops to zero (the insoluble regime), and surface tension will continue to drop during the film compression. However, if this condition is met, surface tension will plateau near γ^*. Thus, changes in cycling frequency can make significant changes in interfacial behavior for this set of conditions.

While we first regarded this phenomenon as a numerical artifact that was corrected by allowing k_1 and k_2 to be continuous functions of the interfacial concentration, Γ, we found that there are physically realistic situations that can exhibit this same phenomenon, even when we allowed k_1 and k_2 to be continuous functions of interfacial surfactant concentration (Eq. (12)). Figure 11 shows an example of this phenomenon, taken from surfactometry data we have previously published using a reconstituted lung surfactant fraction (surfactant first separated into protein and lipid fractions and then recombined [8]). Note that, contrary to the other $\gamma-A$ loops shown here, Fig. 11 shows that decreasing the oscillation

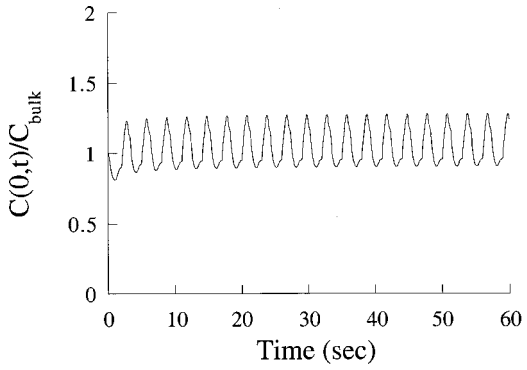

Fig. 10 Predictions for the surfactant concentration in the subsurface region immediately underlying the interface, $C(0,t)$, for the dynamic cycling described in Fig. 9(A) at 20 cycles/min

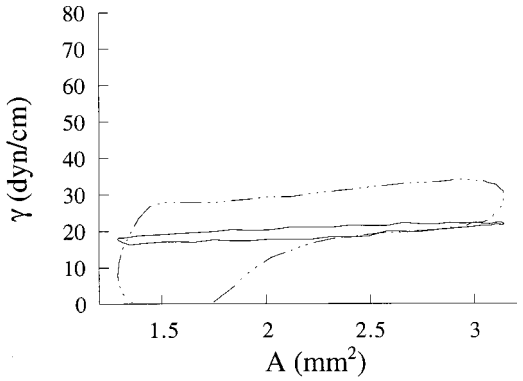

Fig. 11 Experimental data from Ingenito et al. [8] showing steady-state surface tension as a function of interfacial area for reconstituted surfactant at a bulk concentration of 0.1 mg/ml for 1 cycle/min (solid) and 20 cycles/min (dot-dashed). Pseudo-film collapse behavior is seen during the compression phase of the 1 cycle/min loop.

frequency can lead to an increase in minimum surface tension. We hypothesize that this is caused by the pseudo-film collapse phenomenon.

To investigate this process further, we examined how increases in K_2 (see Eqs. (12) and (13)) would affect the shape of the $\gamma - A$ loops at a bulk surfactant concentration of 0.1 mg/ml. This is the concentration of surfactant where the pseudo-film collapse is most often seen in our simulations. Since we hold K_1/K_2 constant (equivalent to holding the equilibrium interfacial surfactant concentration constant, and thus holding the isotherm relating bulk concentration to equilibrium surface tension constant), increasing K_2 necessarily leads to an increase in K_1. Thus, the question we ask is, for a surfactant with equivalent equilibrium surface tension properties to lung surfactant, how would increases in its adsorption rate affect function?

Figure 12 shows that as K_1 is increased from 6 to 100 ml/(g min), the peak surface tension drops, as would be expected. As K_1 is further increased, peak surface tension remains unchanged. However, the area at which the transition to the insoluble regime is observed at progressively smaller areas until at $K_1 = 600$ ml/(g min), the insoluble regime is not reached and the minimum surface tension rises to over 20 dynes/cm.

This pseudo-film collapse is caused by the increased adsorption/desorption rate (equivalent to increased ease of the surfactant molecules moving into and out of the interface) leading to

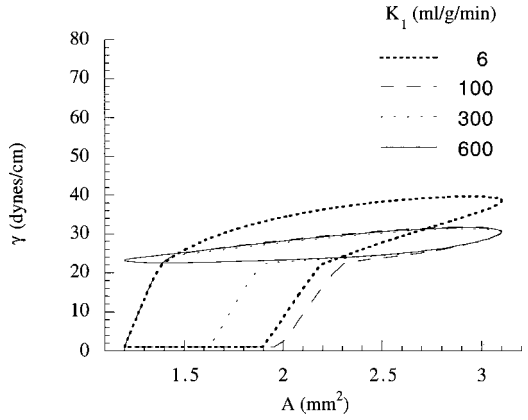

Fig. 12 Steady-state diffusional model predictions of dynamic surface tension as a function of interfacial area at 20 cycles/min at a bulk surfactant concentration of 0.1 mg/ml. K_1/K_2 held constant; other parameters as indicated in the text.

an increased desorption rate for Γ near Γ^*, thus preventing the transition to the insoluble regime that is necessary to achieve near zero surface tension.

Discussion

While our previous adsorption-limited model [7,8] for surfactant exchange to and from an air–liquid interface had the advantage of simplicity and computational speed, we here have found situations in which diffusional transport resistance to and from the interface appears to be limiting the transport rate. Transiently (before steady-state is reached), the adsorption time-scale can be estimated as $1/(K_1 C_{\text{bulk}})$, while the diffusional time-scale is estimated as $(\Gamma^*/C_{\text{bulk}})^2/D$. Using the ratio of these time scales, we can find that the diffusional transport resistance is important for all of the transient conditions we have considered in this paper.

Under steady-state conditions, this balance is altered. While the estimate for the adsorption time scale is the same, the diffusional time scale is now estimated as $1/\omega$ [14]. The ratio of time scales now indicates that the process is still diffusion-limited at high bulk concentrations and low frequencies. However, at high bulk concentration, film collapse controls surfactant kinetics and similar profiles are seen whether the process is assumed to be adsorption-controlled or diffusion-controlled (see Figs. 8(D), 9(A), and 9(D)). Thus, at steady-state cycling conditions, diffusion-limited transport is most relevant at low frequencies (compare Fig. 8(F) to Figs. 9(C) and 9(F)) and low bulk concentration.

As diffusional transport resistance is most important transiently, it is not surprising that we could not match the surface tension/interfacial area loops presented by Schürch et al. [3] with our previous adsorption-limited model. They conducted experiments in which a bubble was freshly formed and surface tension versus time was monitored (Fig. 2(A)); then dynamic cycling was begun (Figs. 3(A–C)), and after 1, 20, or 50 cycles, the cycling was stopped at maximum bubble volume and surface tension versus time was again monitored (Fig. 4(A)). While we were able to find model parameters that matched each of the experiments, different values of these parameters were required to match the different experiments even through the same surfactant preparation was used. Specifically, the parameter values required to match Fig. 2(A) ($D = 1\times10^{-6}$ cm^2/s and $K_1 = 6\times10^5$ ml/g/min) were similar to those that matched our steady-state oscillations of calf lung surfactant in a pulsating bubble surfactometer (Figs. 9(A–C)). The parameter values necessary to match Figs. 3(A–C) and Fig. 4(A) ($D = 1\times10^{-9}$ cm^2/s and $K_1 = 0.07\times10^5$ ml/g/min) on the other hand are two to three orders of magnitude lower and thus suggest much higher transport resistance. This can be seen qualitatively by comparing Fig. 2(A) to Fig. 4(A): it is clear that it takes much longer for surfactant to reabsorb to the bubble after it has been cycled (Fig. 4(A)) than when the bubble is first formed (Fig. 2(A)).

We postulate that this increased transport resistance originates from the high level of compression (80 percent) that occurs at the beginning of the first cycle after the bubble interface has been saturated with surfactant. As the interface is known to be enriched in DPPC [19,20] high compression and the resulting ejection of interfacial material would be expected to lead to a great enrichment of DPPC in the subsurface region, and thus alter the transport properties of surfactant in this region. In fact, the value of K_1 that we find to match the Schürch et al. data, $K_1 = 0.07\times10^5$ ml/g/min, is in very good agreement with previous studies that we have conducted on DPPC [8]. The diffusion coefficient that matches these data, $D = 1\times10^{-9}$ cm^2/s, is consistent with that of very, very large micelles or lamellar bodies, structures that DPPC is known to form [21].

Using the parameters that matched the oscillatory data of Schürch et al., our model predicts that a high concentration subsurface layer of surfactant will form (see Fig. 6). This substantial depot has been visualized by other investigators [9] and Schürch

et al. postulated that ''. . . a new phase of unknown structure (collapse phase) probably consisting of bilayers or higher-order multilayers may form, which determines, to a greater extent, the surface activity of the film in the ensuing curve'' [3]. Figures 6 and 7 support this conjecture. This high concentration of surfactant in the subphase equilibrates only slowly with the bulk.

Our model predicts this subsurface layer to be quite thin (Fig. 6), relative to the bubble size. This ameliorates two possible modeling concerns, namely, the stir-bar that is used to mix the bulk solution in the captive bubble surfactometers [6], and the nonspherical geometry of the bubbles in that system [6,22]. The thin concentration boundary layer (see Fig. 7) indicates that the Reynolds number in this region will be tiny, and thus mixing due to the stir-bar will not influence transport in the region of the bubble. Furthermore, the thin concentration boundary layer means that transport is largely planar in the region of the bubble and only weakly affected by bubble geometry.

This subsurface layer of surfactant is predicted to contain much less mass in our steady-state oscillations of calf lung surfactant in a pulsating bubble surfactometer (PBS) (Fig. 10). This is due to the more rapid adsorption (much larger values of K_1) that we found best matched that data. We attributed this difference from the Schürch et al. data to the significant squeeze-out caused by the high compression level used in those experiments (80 percent). The PBS also significantly compresses the interface (by approximately 58 percent), but this likely leads to a lesser enrichment of DPPC in the subsurface region than in Schürch's experiments. Furthermore, there is a very significant difference in initial conditions between the experiments done with a PBS and those done by Schürch et al. using a captive bubble surfactometer. While Schürch et al. begin their experiments at maximum bubble volume, with the bubble saturated with surfactant, the PBS experiments begin with a minimum bubble volume. Thus, in the experiments conducted with the PBS, the experiment begins with less total surfactant in the interface. A further difference between the two experimental conditions involves the possibility of surfactant leakage along the tube that has been noted during transient behavior with a PBS [18].

While the extension of our previous model to include diffusional transport resistance was crucial to be able to match the data of Schürch et al., it also gave better matches to the steady-state oscillatory data in the PBS. The experimental data at low bulk concentration (Fig. 8(C)) was better matched by the new model (Fig. 9(C)) as opposed to our previous adsorption-limited model (Fig. 8(F)).

Finally, use of the extended model allowed us to identify a phenomenon that we have termed ''pseudo-film collapse.'' While this is not intrinsic to a diffusional model, the detailed characterization of the spatial variations of surfactant concentration, particularly near the interface, allowed the phenomenon to be more readily seen. The importance of recognizing the possibility of ''pseudo-film collapse'' is that the observation of a relatively constant surface tension at γ near γ^* with decreasing interfacial area does not necessarily imply that film collapse is occurring. It may indicate a surfactant with a high desorption coefficient.

This is likely an important consideration in the design of surfactant replacements. While a goal of increasing surfactant adsorption rate has been generally pursued because of the known problem with the low adsorption rate of DPPC, ''pseudo-film collapse'' indicates that adsorption rates that are too high might also be problematic. Increasing adsorption rate is generally to be expected to increase desorption rate; in our experience, these two rate constants have always been linked [7,8]. Thus, increasing the adsorption rate can lead to an increased desorption rate and, potentially, ''pseudo-film collapse.'' This may provide an important constraint for design of surfactant replacements.

In summary, we have extended our model for surfactant transport to and from an oscillating interface. The addition of diffusion to the model allowed matching to transient data and better agreement between model and data for steady-state oscillatory data. While there are a number of situations in which the extended model gives significantly improved predictions, steady-state oscillatory data at high bulk concentration is still adequately modeled by an adsorption-limited model, which is computationally more efficient.

Acknowledgments

This work was supported by NIH grant No. P01 HL33009 and by an NSF Fellowship to J. Morris.

References

[1] Fuchimukai, T., Fujiwara, T., Takahashi, A., and Enhorning, G., 1987, ''Artificial Pulmonary Surfactant Inhibited by Proteins,'' J. Appl. Physiol., **62**, pp. 429–437.
[2] Holm, B. A., Venkitaraman, A. R., Enhorning, G., and Notter, R. H., 1990, ''Biophysical Inhibition of Synthetic Lung Surfactants,'' Chem. Phys. Lipids, **52**, pp. 243–250.
[3] Schürch, S., Schurch, D., Curstedt, T., and Robertson, B., 1994, ''Surface Activity of Lipid Extract Surfactant in Relation to Film Area Compression and Collapse,'' J. Appl. Physiol., **77**, pp. 974–986.
[4] Wang, Z., Hall, S. B., and Notter, R. H., 1995, ''Dynamic Surface Activity of Films of Lung Surfactant Phospholipids, Hydrophobic Proteins, and Neutral Lipids,'' J. Lipid Res., **36**, pp. 1283–1293.
[5] Enhorning, G., 1977, ''Pulsating Bubble Technique for Evaluating Pulmonary Surfactant,'' J. Appl. Physiol., **43**, pp. 198–203.
[6] Schürch, S., Bachofen, H., Goerke, J., and Possmayer, F., 1989, ''A Captive Bubble Method Reproduces the in Situ Behavior of Lung Surfactant Monolayers,'' J. Appl. Physiol., **67**, pp. 2389–2396.
[7] Otis, Jr., D. R., Ingenito, E. P., Kamm, R. D., and Johnson, M., 1994, ''Dynamic Surface Tension of Surfactant TA: Experiments and Theory,'' J. Appl. Physiol., **77**, pp. 2681–2688.
[8] Ingenito, E. P., Mark, L., Morris, J., Espinosa, F. F., Kamm, R. D., and Johnson, M., 1999, ''Biophysical Characterization and Modeling of Lung Surfactant Components,'' J. Appl. Physiol., **86**, pp. 1702–1714.
[9] Tchoreloff, P., Gulik, A., Denizot, B., Proust, J. E., and Puisieux, F., 1991, ''A Structural Study of Interfacial Phospholipid and Lung Surfactant Layers by Transmission Electron Microscopy After Blodgett Sampling: Influence of Surface Pressure and Temperature,'' Chem. Phys. Lipids, **59**, pp. 151–165.
[10] Notter, R. H., Tabak, S. A., Holcomb, S., and Mavis, R. D., 1980, ''Postcollapse Dynamic Surface Pressure Relaxation in Binary Surface Films Containing Dipalmitoyl Phosphatidylcholine,'' J. Colloid Interface Sci., **74**, pp. 370–377.
[11] Smith, R. D., and Berg, J. C., 1980, ''The Collapse of Surfactant Monolayers at the Air–Water Interface,'' J. Colloid Interface Sci., **74**, pp. 273–286.
[12] Chang, D. H., and Franses, E. I., 1994, ''Dynamic Tension Behavior of Aqueous Octanol Solutions Under Constant-Area and Pulsating-Area Conditions,'' Chem. Eng. Sci., **49**, pp. 313–325.
[13] Otis, D., 1994, *An Investigation of the Mechanisms Responsible for Pulmonary Airway Closure*, Mechanical Engineering, Cambridge, MIT, p. 203.
[14] Morris, J., 1998, ''Characterization of the Dynamic Behavior of Lung Surfactant and Its Components,'' Mechanical Engineering, MIT, Cambridge, MA.
[15] Patankar, S. V., 1980, *Numerical Heat Transfer and Fluid Flow*, Hemisphere, New York.
[16] Press, W. H., Teukolsky, S. A., Vetterling, W. T., and Flannery, B. P., 1992, *Numerical Recipes in FORTRAN. The Art of Scientific Computing*, Cambridge University Press, Cambridge, U.K.
[17] Johannsen, E. C., Chung, J. B., Chang, C. H., and Franses, E. I., 1991, ''Lipid Transport to Air/Water Interfaces,'' Colloids Surface, **53**, pp. 117–134.
[18] Putz, G., Goerke, J., Taeusch, H. W., and Clements, J. A., 1994, ''Comparison of Captive and Pulsating Bubble Surfactometers With Use of Lung Surfactants,'' J. Appl. Physiol., **76**, pp. 1425–1431.
[19] Schürch, S., Qanbar, R., Bachofen, H., and Possmayer, F., 1995, ''The Surface-Associated Surfactant Reservoir in the Alveolar Lining,'' Biol. Neonate, **67** (Suppl.), pp. 61–76.
[20] Schürch, S., Green, F. H. Y., and Bachofen, H., 1998, ''Formation and Structure of Surface Films: Captive Bubble Surfactometry,'' Biochim. Biophys. Acta, **1408**, pp. 180–202.
[21] Tanford, C., 1973, *The Hydrophobic Effect*, Wiley-Interscience, New York.
[22] Hall, S. B., Bermel, M. S., Ko, Y. T., Palmer, H. J., Enhorning, G., and Notter, R. H., 1993, ''Approximations in the Measurement of Surface Tension on the Oscillating Bubble Surfactometer,'' J. Appl. Physiol., **75**, pp. 468–477.